



Supplement of

Recommended coupling to global meteorological fields for long-term tracer simulations with WRF-GHG

David Ho et al.

Correspondence to: David Ho (tzuho@bgc-jena.mpg.de)

The copyright of individual parts of the supplement might differ from the article licence.

FDLR in-situ / 20180529a / WRF-GHG

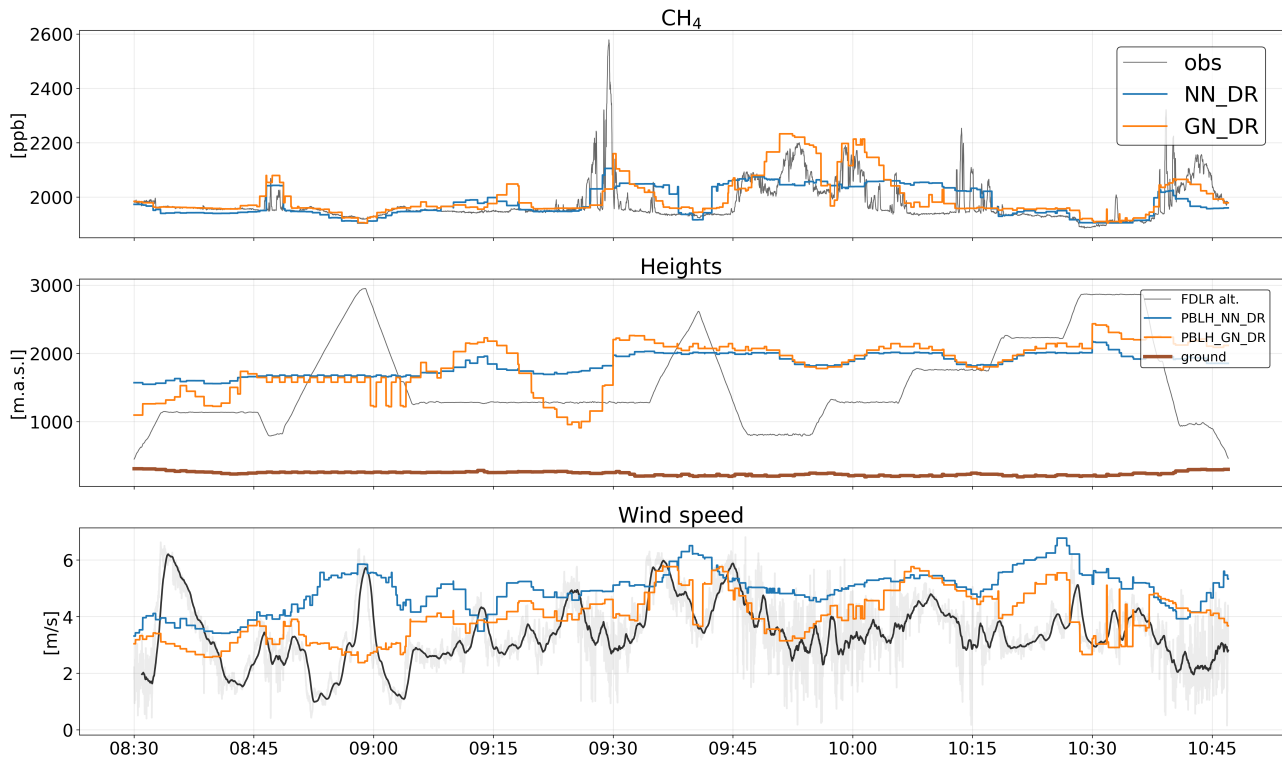


Figure S1. Overview time series, showing modeled and observed CH₄ (top), altitude of the aircraft, model-simulated PBLH (middle), and wind speeds (bottom) for flightcode 20180529a

FDLR in-situ / 20180601a / WRF-GHG

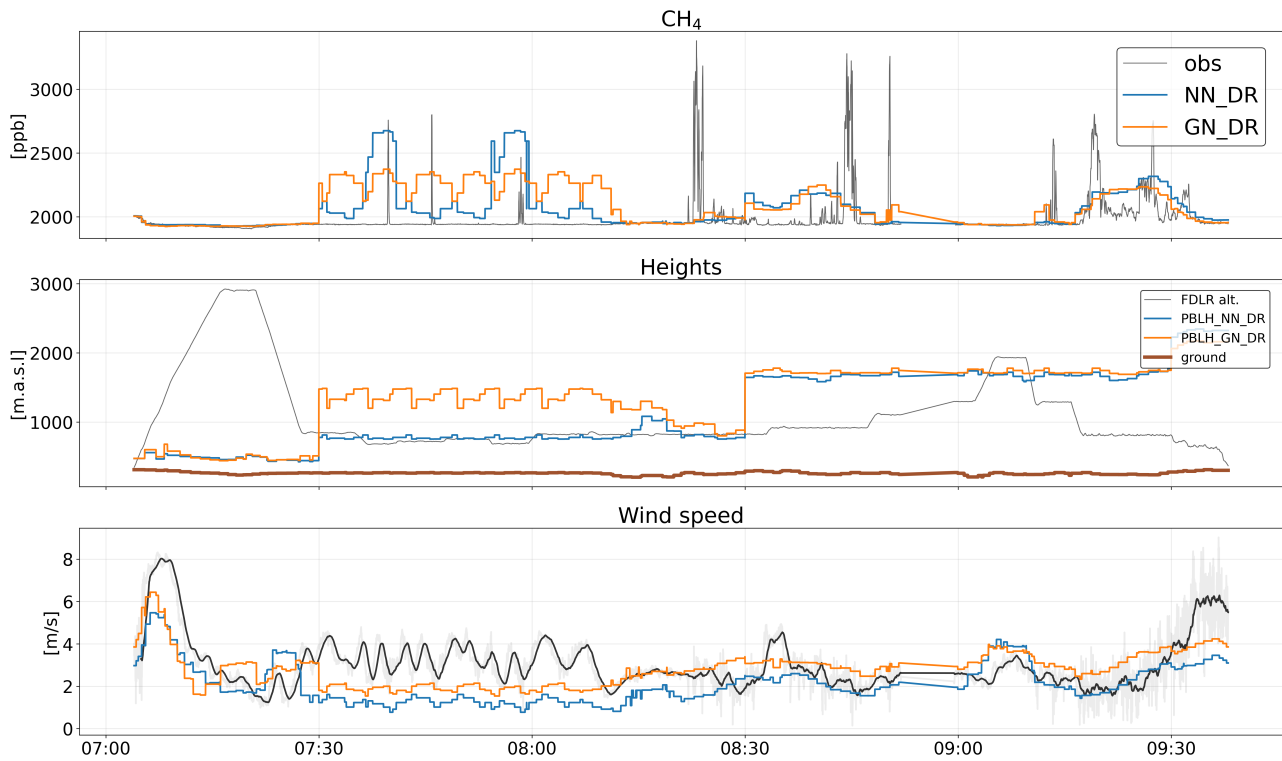


Figure S2. Same as Fig. S1 but for flightcode 20180601a

FDLR in-situ / 20180605a / WRF-GHG

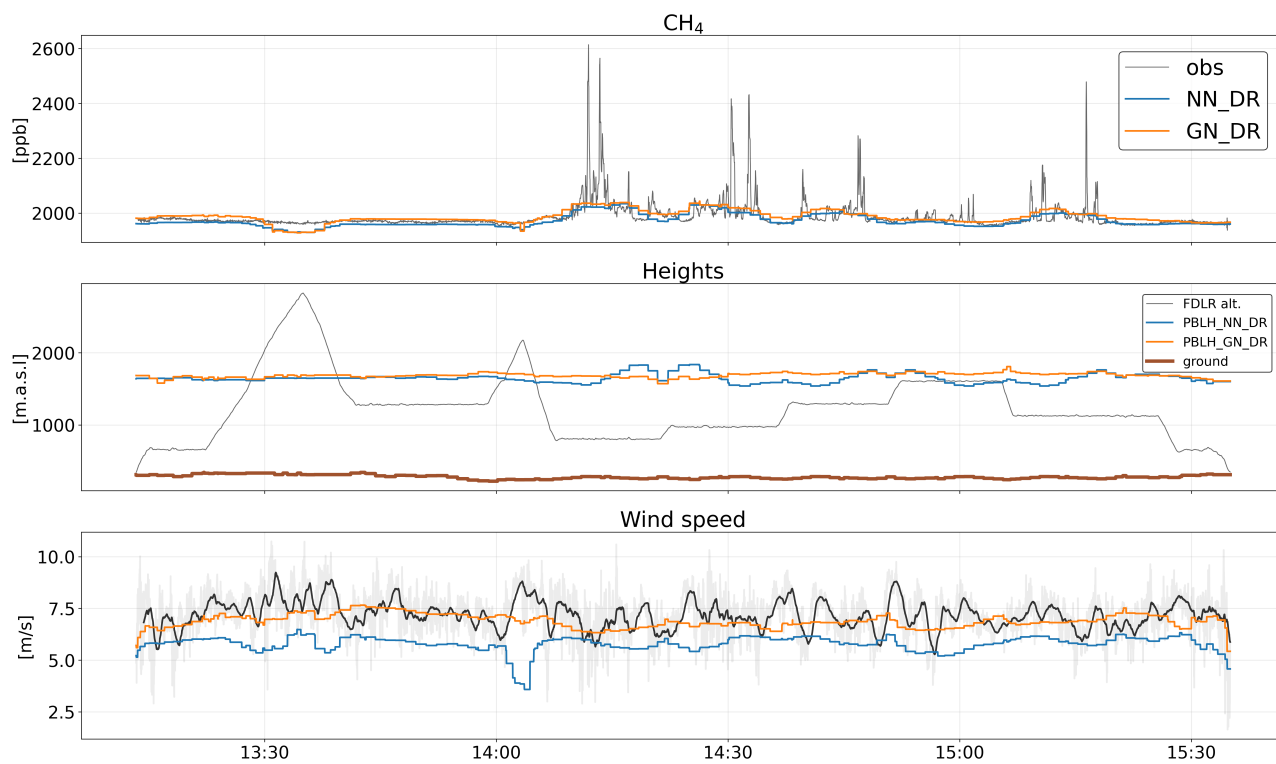


Figure S3. Same as Fig. S1 but for flightcode 20180605a

FDLR in-situ / 20180606a / WRF-GHG

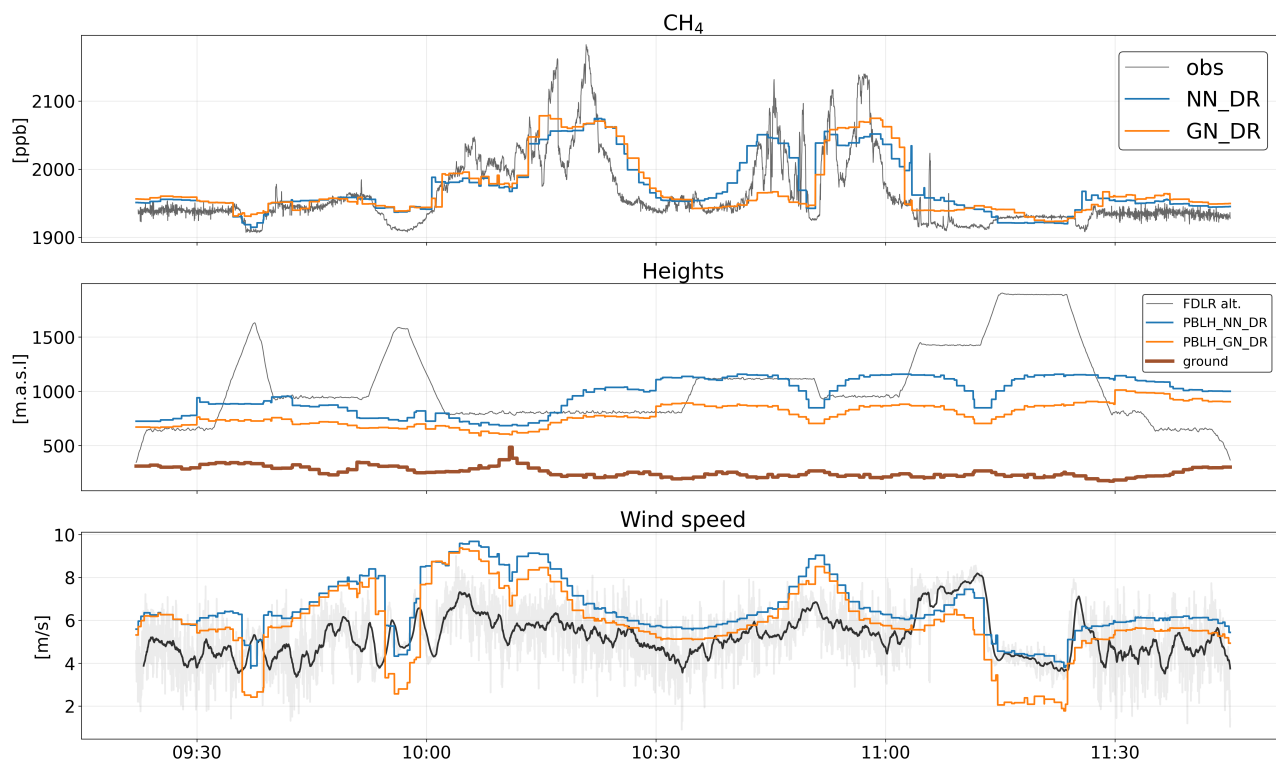


Figure S4. Same as Fig. S1 but for flightcode 20180606a

FDLR in-situ / 20180606b / WRF-GHG

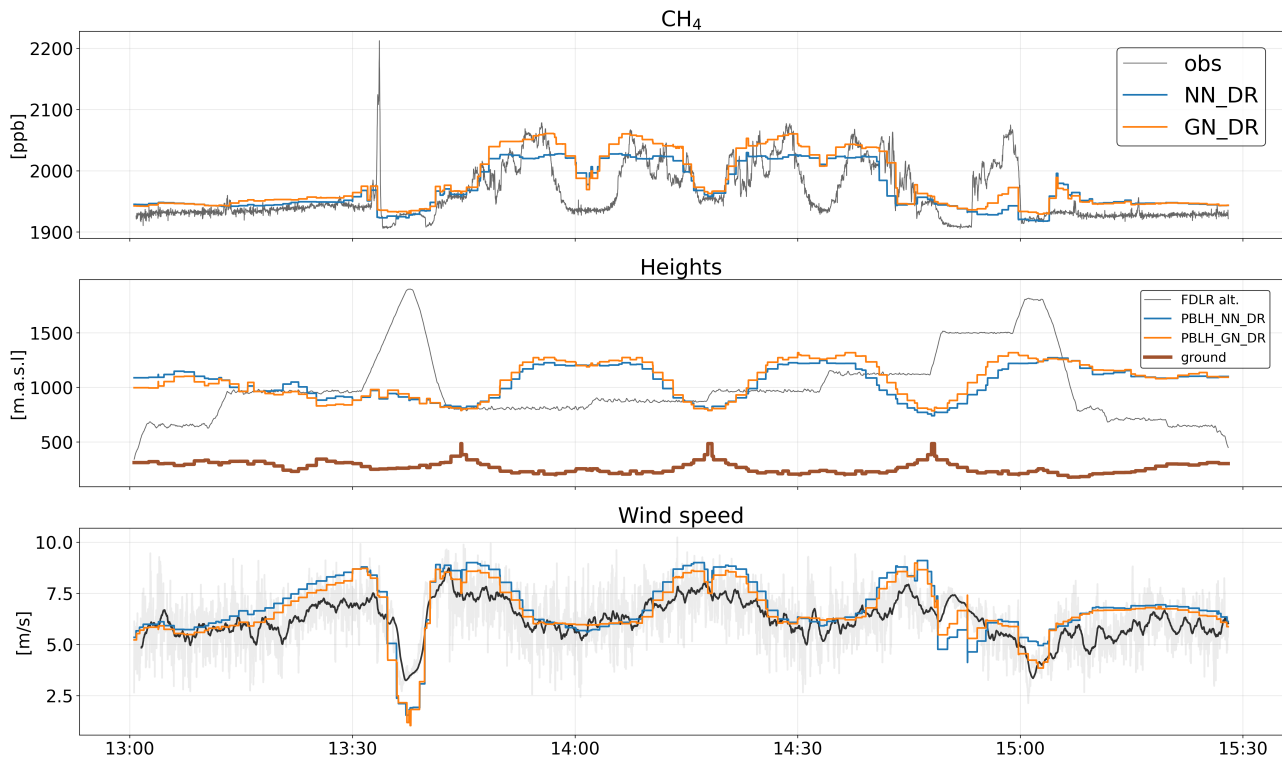


Figure S5. Same as Fig. S1 but for flightcode 20180606b

FDLR in-situ / 20180607a / WRF-GHG

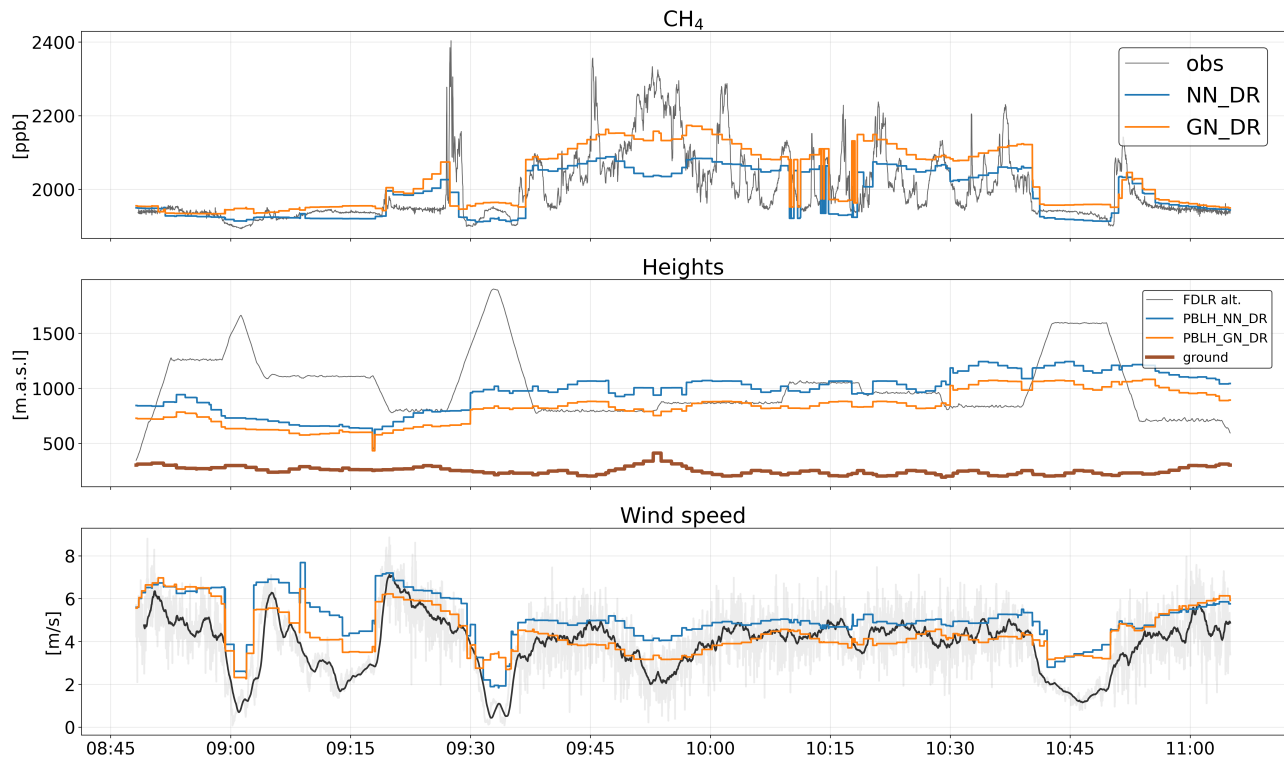


Figure S6. Same as Fig. S1 but for flightcode 20180607a

FDLR in-situ / 20180607b / WRF-GHG

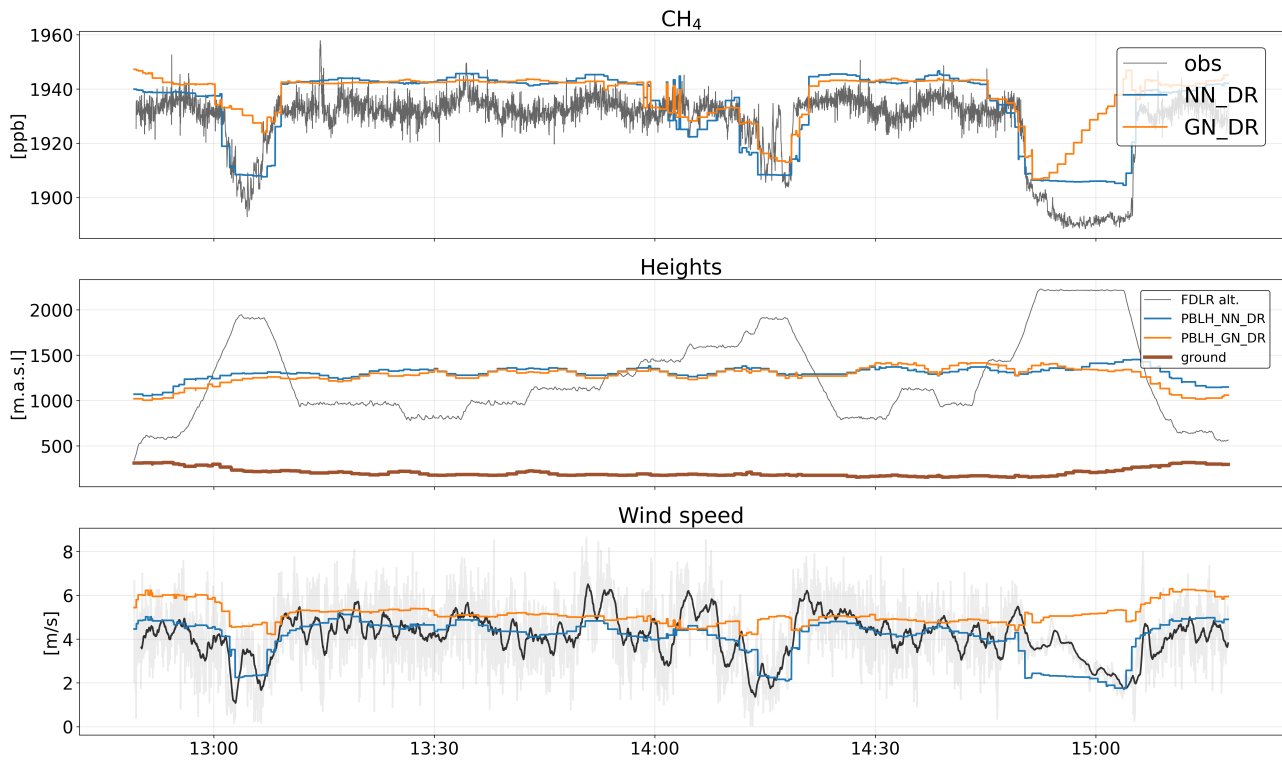


Figure S7. Same as Fig. S1 but for flightcode 20180607b

FDLR in-situ / 20180609a / WRF-GHG

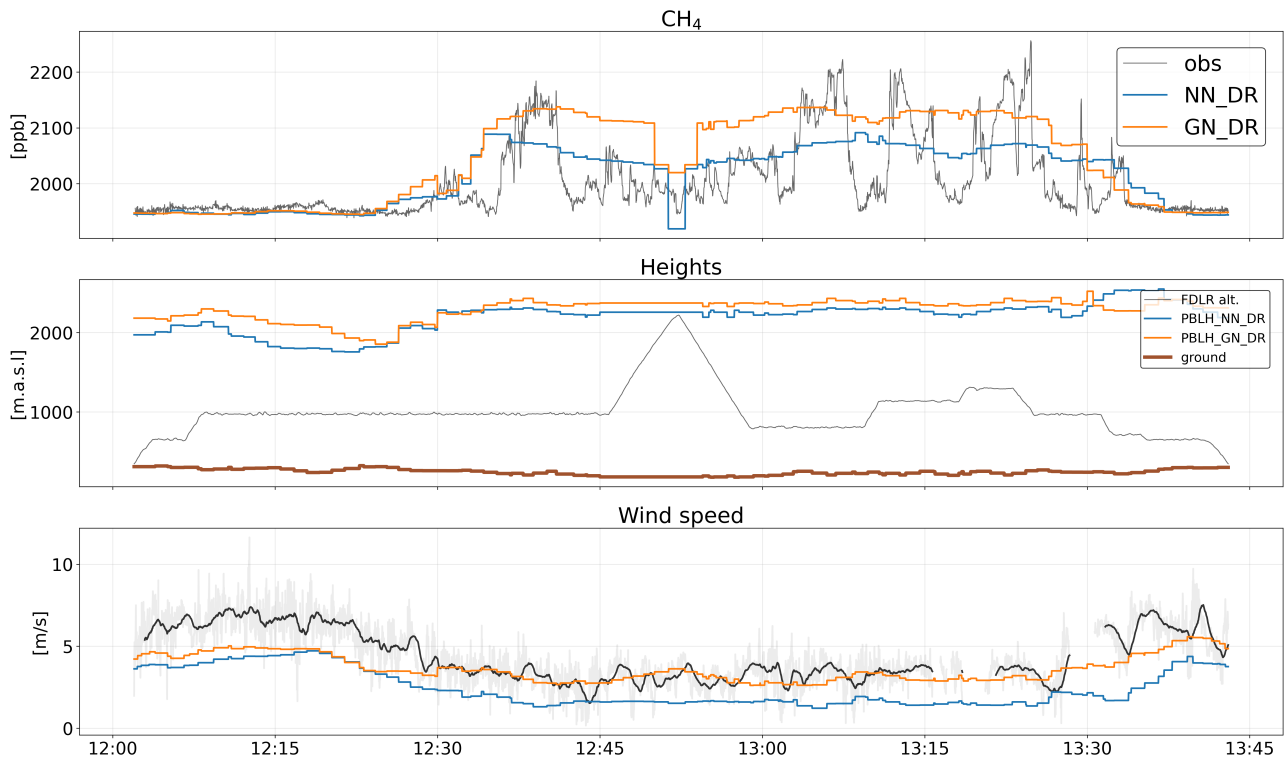


Figure S8. Same as Fig. S1 but for flightcode 20180609a

FDLR in-situ / 20180611a / WRF-GHG

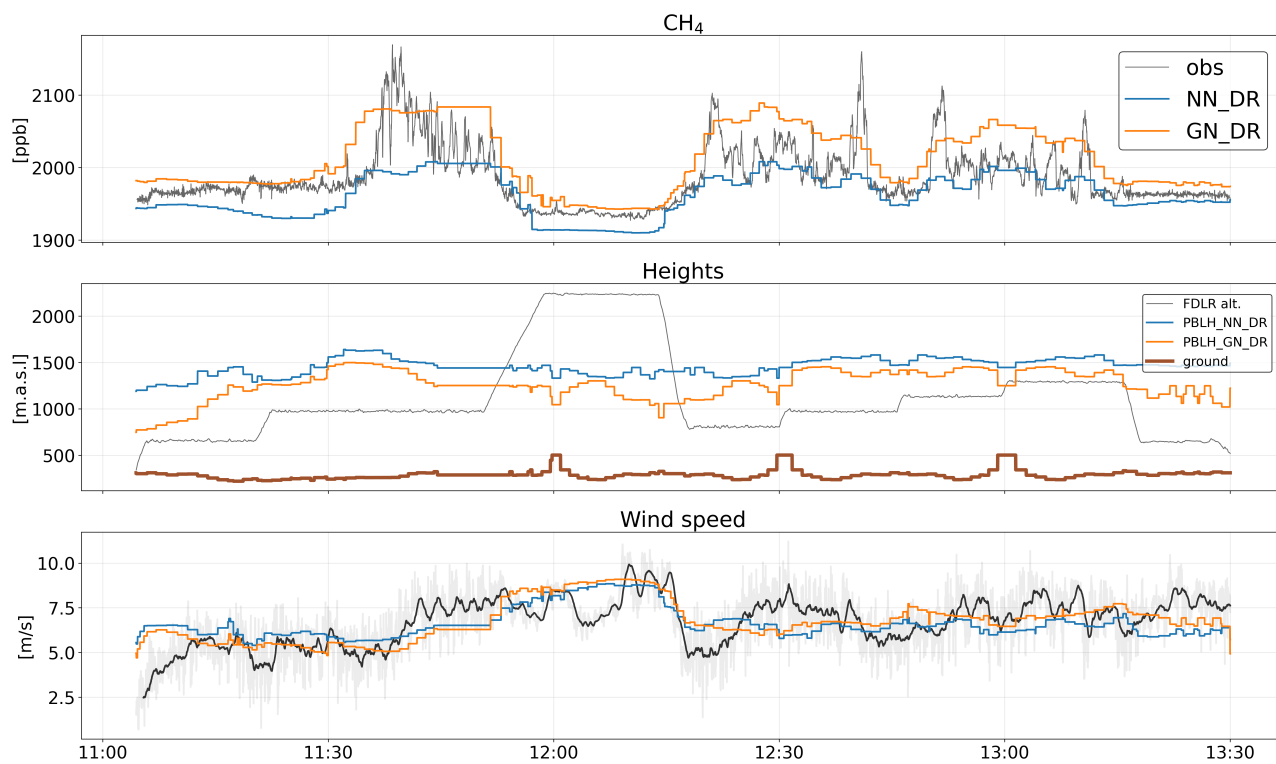


Figure S9. Same as Fig. S1 but for flightcode 20180611a

FDLR in-situ / 20180613a / WRF-GHG

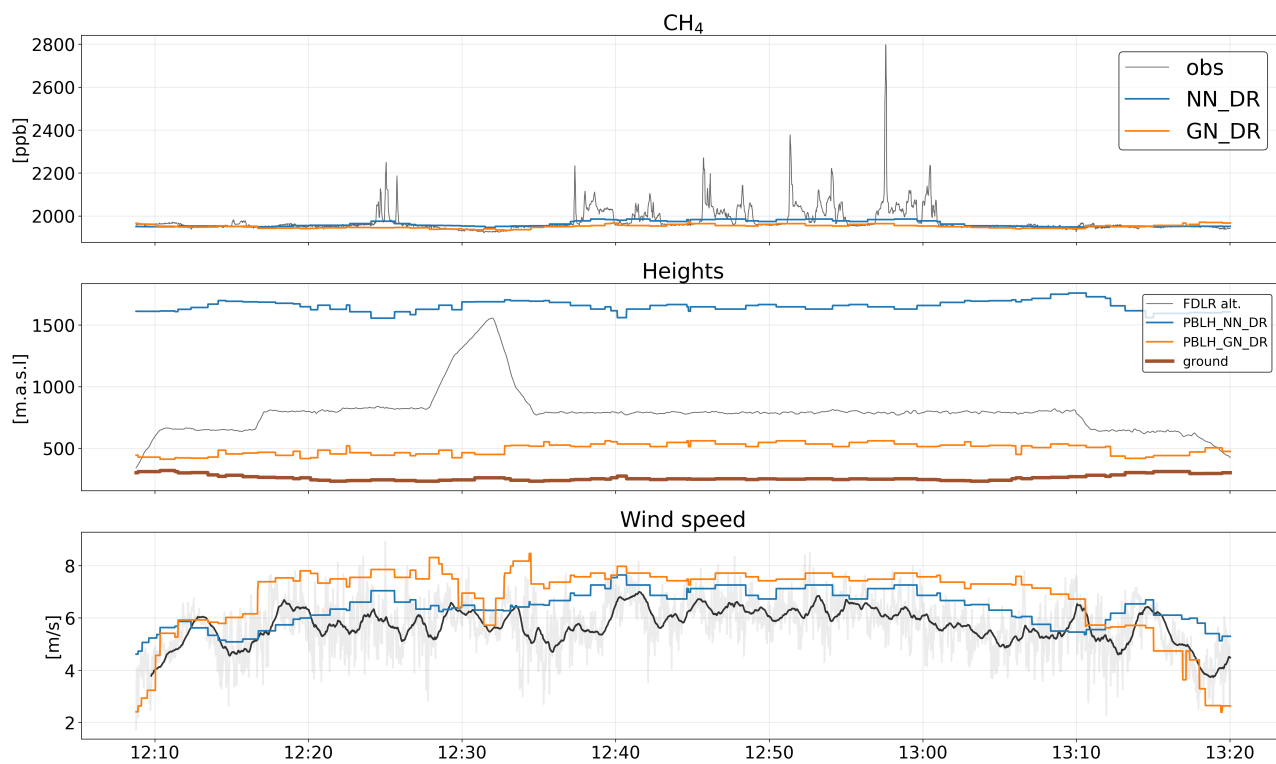


Figure S10. Same as Fig. S1 but for flightcode 20180613a

FDLR in-situ / 20180614a / WRF-GHG

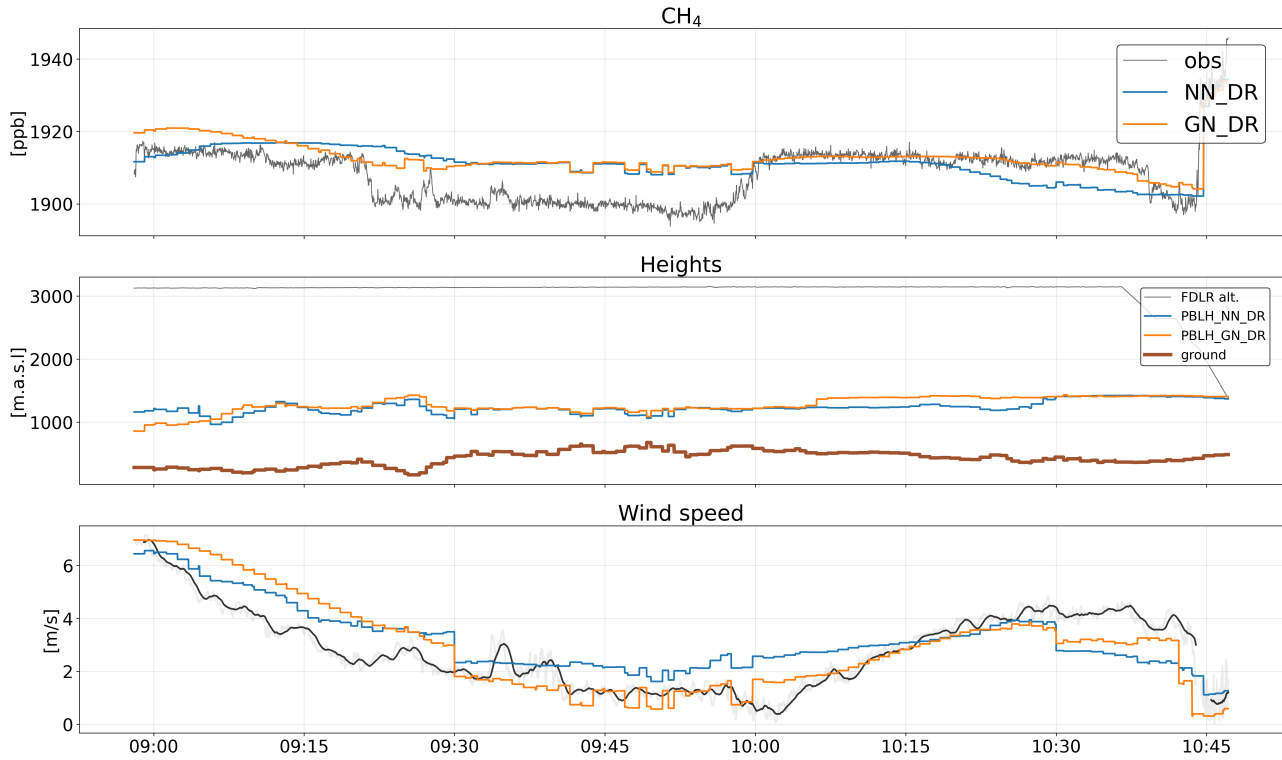


Figure S11. Same as Fig. S1 but for flightcode 20180614a

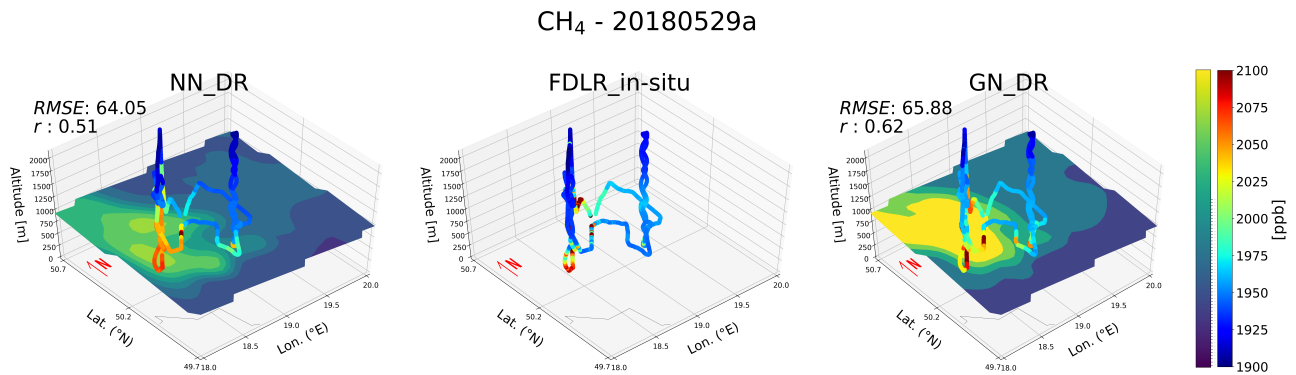


Figure S12. Flight tracks of the airborne platform coloured based on either modelled CH_4 mole fractions (left: NN_DR; right: GN_DR) or in situ aircraft measurements (middle) performed over the Upper Silesian Coal Basin. In situ observation have a high temporal resolution of 1 s spanning about 2.5 hours (ca. 9000 time steps), the models fields were stored hourly. Modeled values were extracted along the flight track from the nearest point in time and space. 2-D planes of the modeled CH_4 at a model level ca. 950 m.a.s.l. are also plotted to give an indication of the plume structure and the location of the point source.

CH₄ - 20180601a

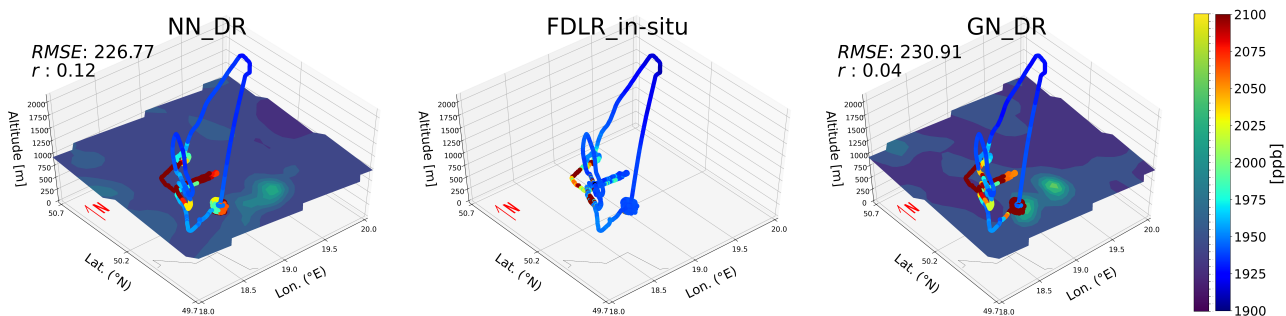


Figure S13. Same as Fig. S12 but for flightcode 20180601a. The main target was Pniówek Center shaft. The aircraft was spiraling around the point source, the horizontal distance from the source to the spiral loop for both flights were < 5 km.

CH₄ - 20180605a

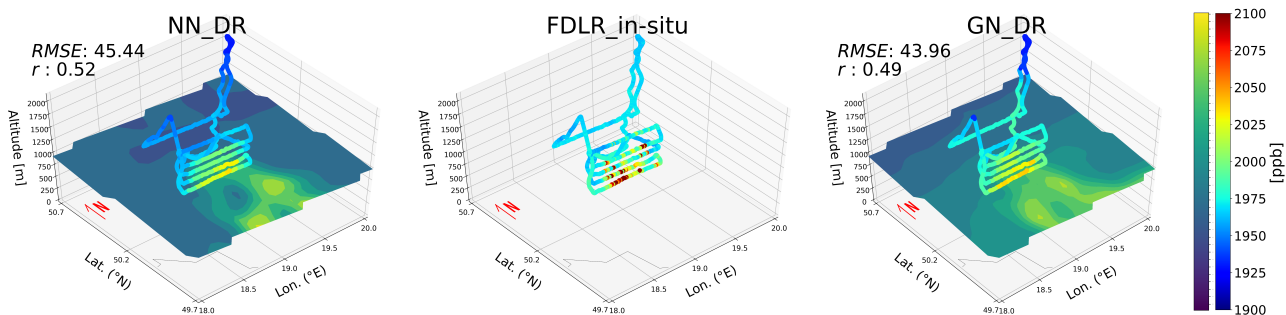


Figure S14. Same as Fig. S12 but for flightcode 20180605a

CH₄ - 20180606a

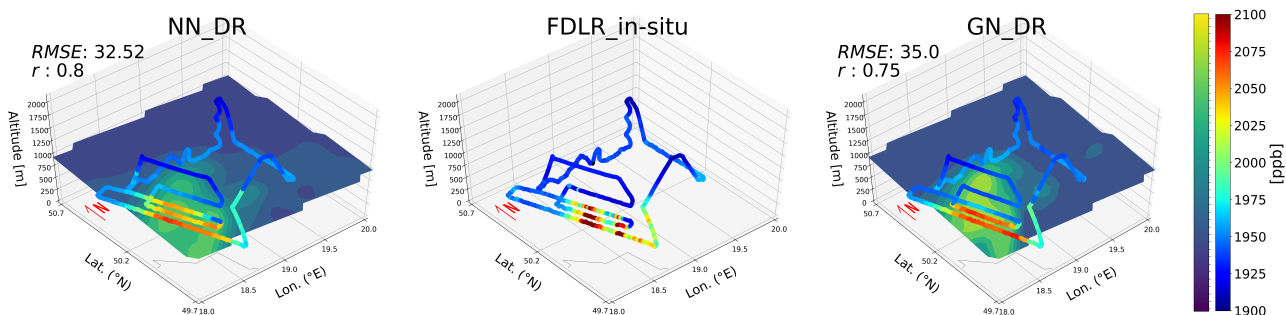


Figure S15. Same as Fig. S12 but for flightcode 20180606a

CH₄ - 20180606b

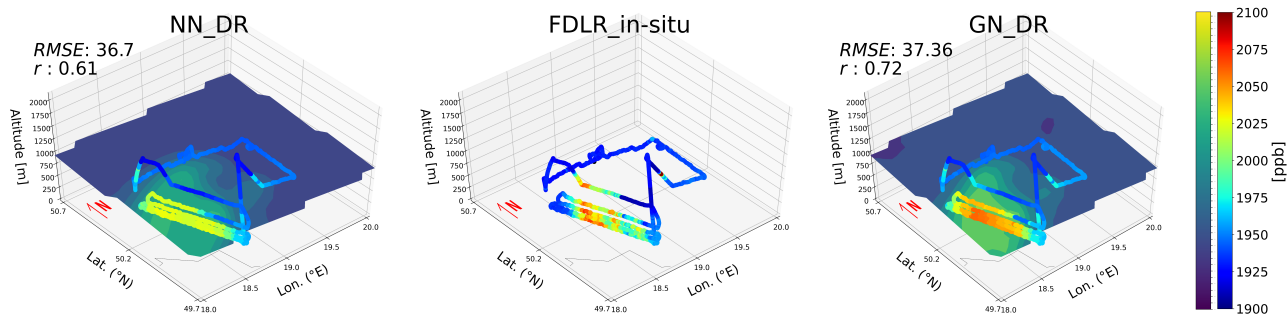


Figure S16. Same as Fig. S12 but for flightcode 20180606b

CH₄ - 20180607a

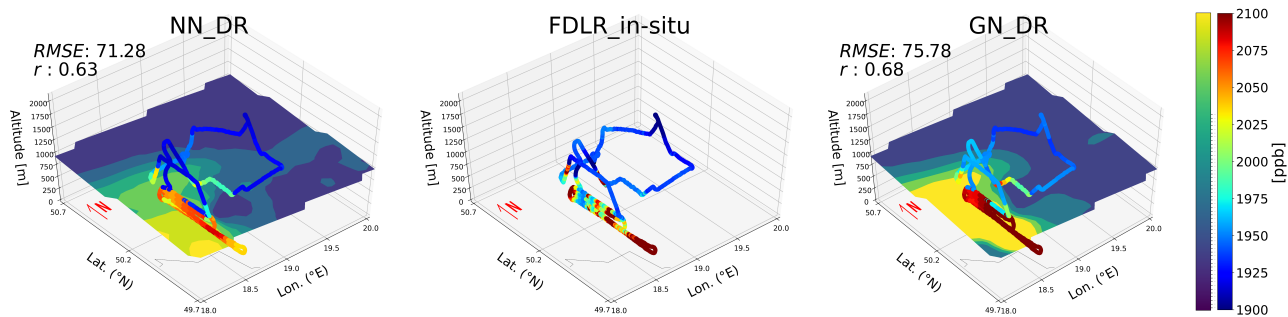


Figure S17. Same as Fig. S12 but for flightcode 20180607a

CH₄ - 20180607b

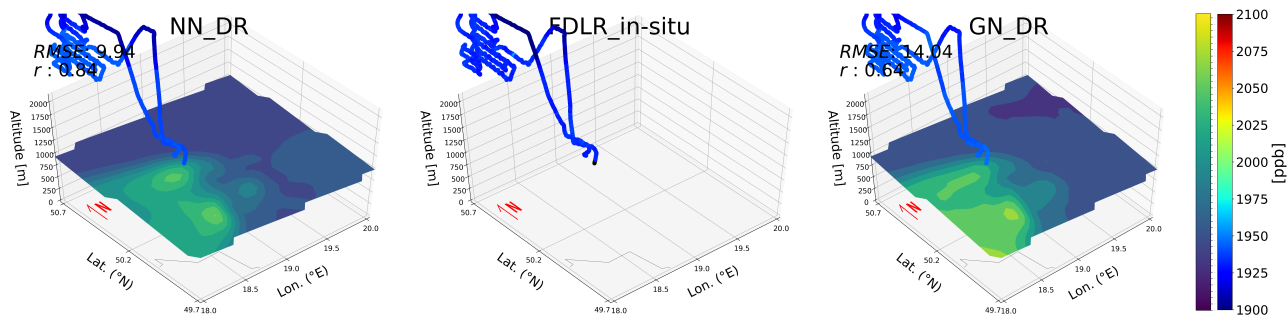


Figure S18. Same as Fig. S12 but for flightcode 20180607b. It was a flight targeted to the Bełchatów power plant (approximately 80 km north away from USCB).

CH₄ - 20180609a

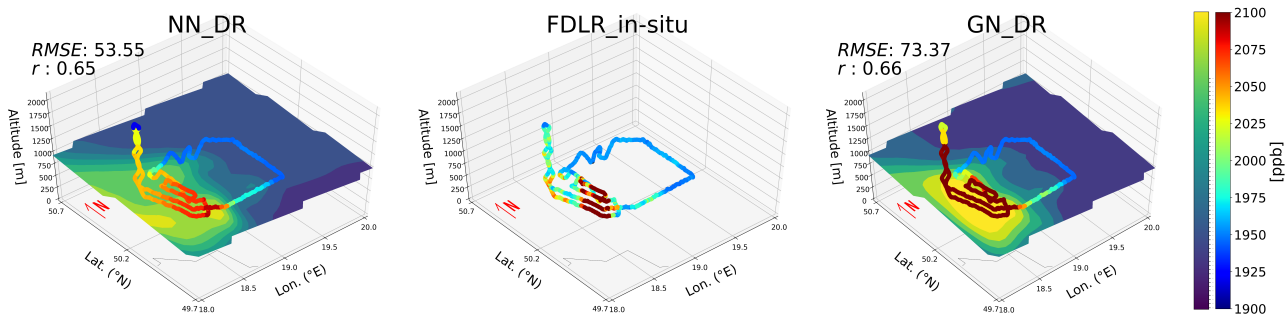


Figure S19. Same as Fig. S12 but for flightcode 20180609a

CH₄ - 20180611a

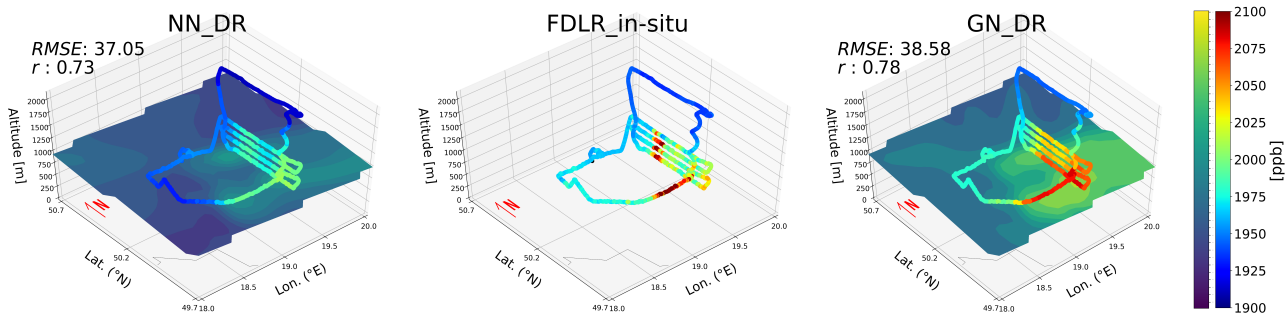


Figure S20. Same as Fig. S12 but for flightcode 20180611a

CH₄ - 20180613a

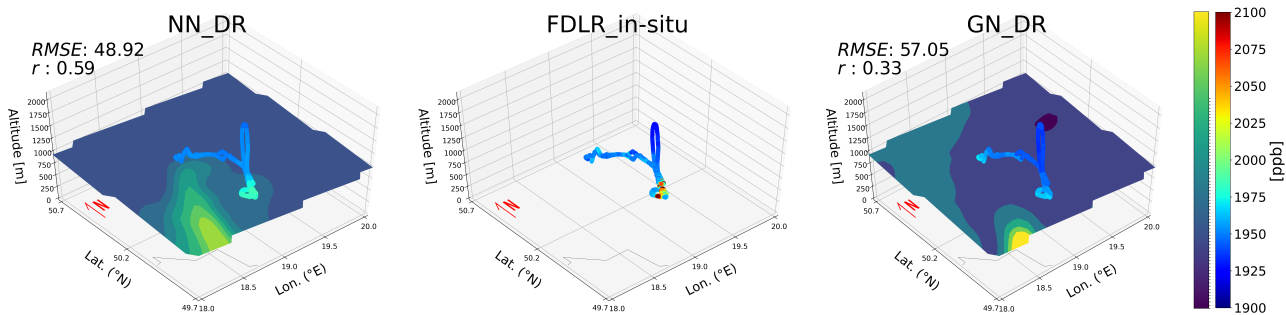


Figure S21. Same as Fig. S12 but for flightcode 20180613a. The main target was shaft Silesia V. The aircraft was spiraling around the point source, the horizontal distance from the source to the spiral loop for both flights were < 5 km.

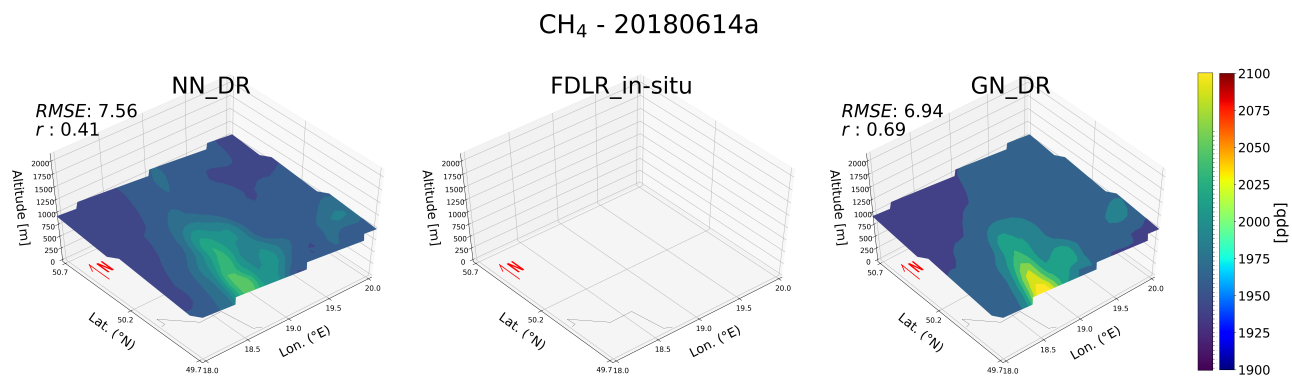


Figure S22. Same as Fig. S12 but for flightcode 20180614a; it was a transfer flight back to Munich (most measurements are above the PBL, 3000 m.a.s.).

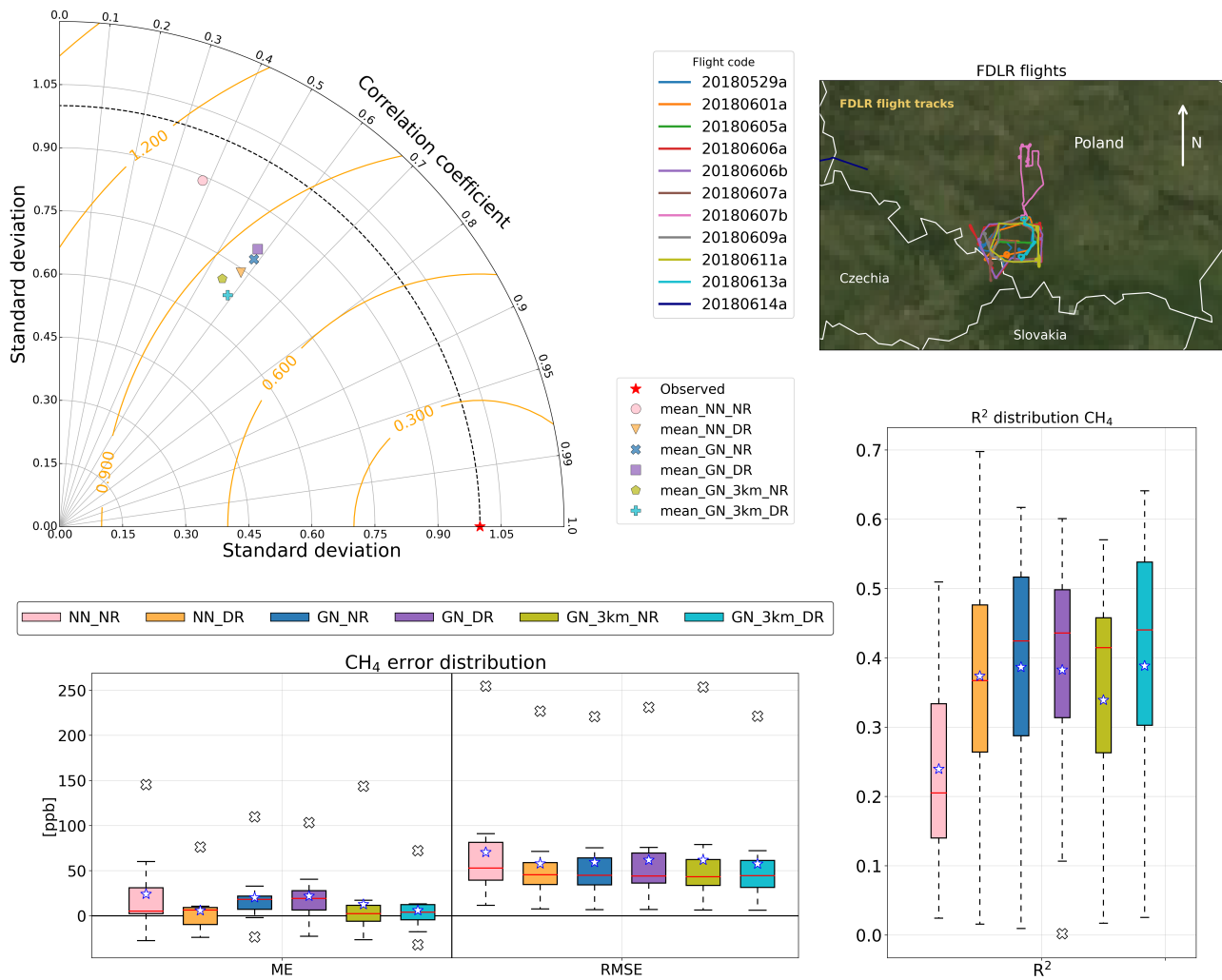


Figure S23. Statistical overview of all flights

CH₄ @Munich (48.08, 11.28)

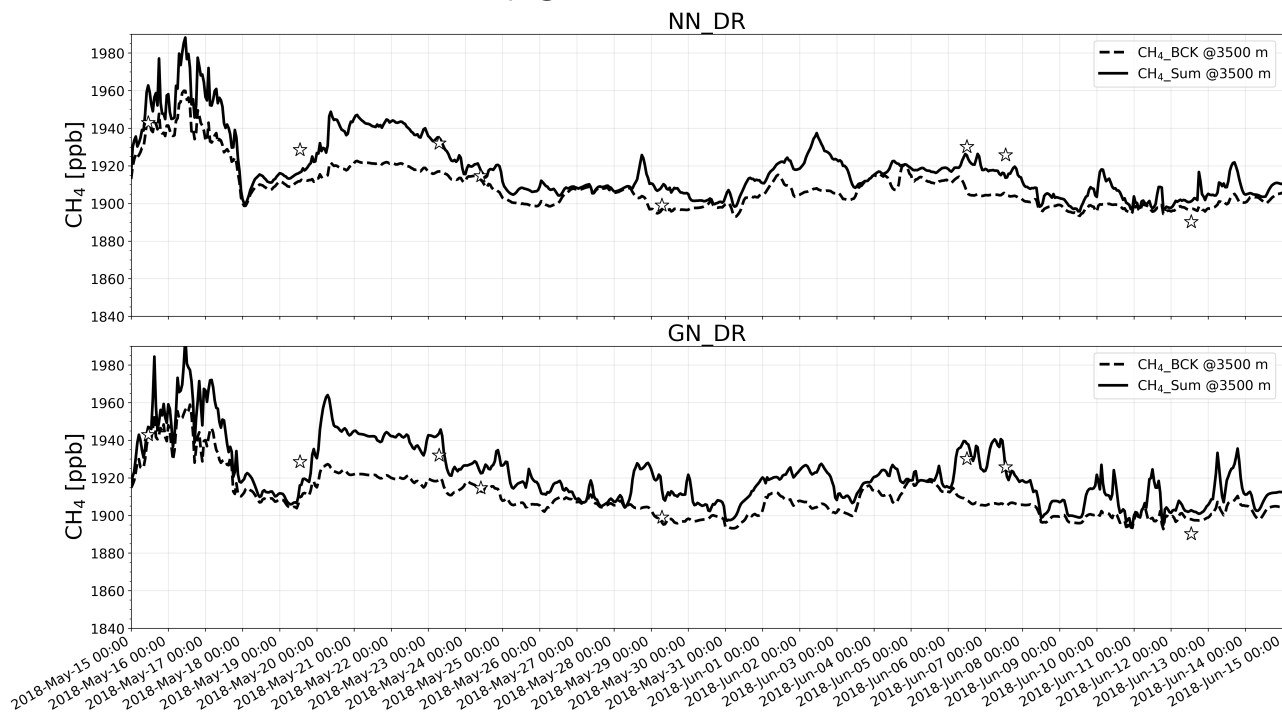


Figure S24. CH₄ (top: NN_DR; bottom: GN_DR) over time at Munich (48.08 °N, 11.28 °E) in mole fraction (ppb). Background methane as CH₄_BCK (dashed lines) and total methane as CH₄_Sum, i.e. the sum of background and anthropogenic CH₄ (solid lines) at 3500 m.a.s.l. The white stars show coincident aircraft-based in situ measurements in the free troposphere.

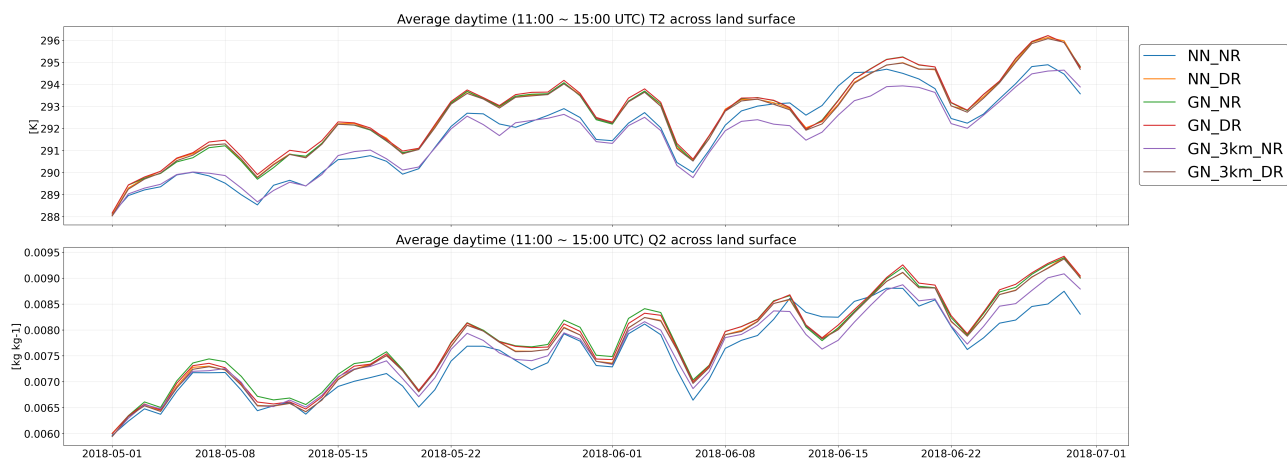


Figure S25. Average daytime (11:00 - 15:00 UTC) Q2 (top) and T2 (bottom) over land within the model domain for different model scenarios between May 1 - June 31, 2018.

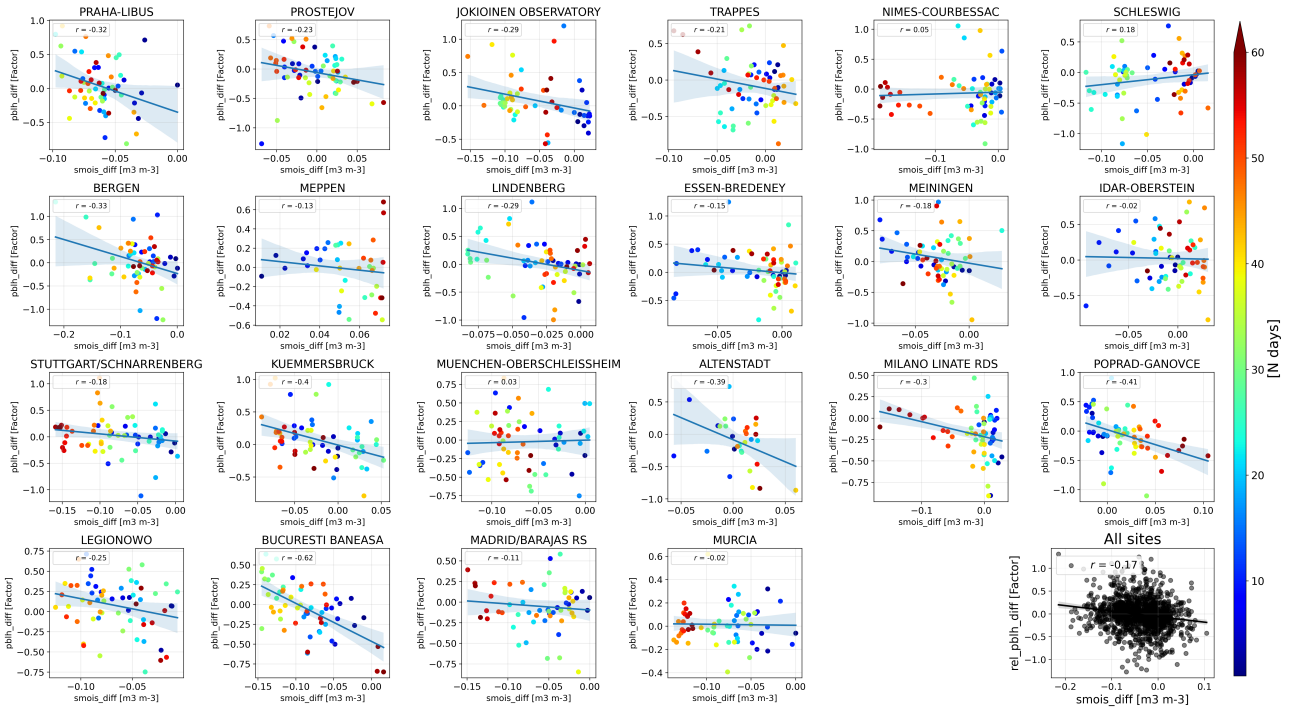


Figure S26. Scatter plot showing the correlation of the difference in SMOIS against the relative difference in PBLH between simulation GN_DR and NN_NR at 22 different locations. The colors mark the day after 1 May (61 days in total up to 1 July) from blue to red. The plot in the lower right corner contains the data collected from all 22 sites.

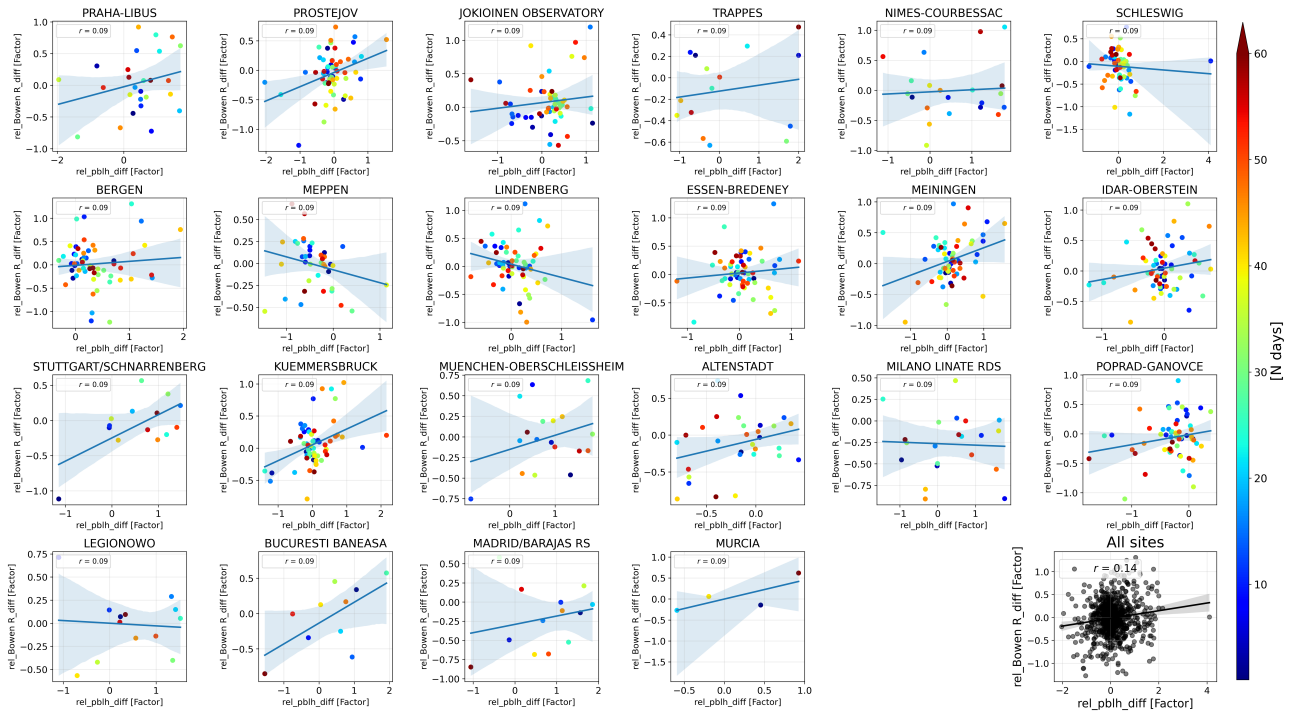


Figure S27. Scatter plot showing the correlation of the relative difference in PBLH against the relative difference in Bowen Ratio between simulation GN_DR and NN_NR at 22 different locations. The colors mark the day after 1 May (61 days in total up to 1 July) from blue to red. The plot in the lower right corner contains the data collected from all 22 sites.

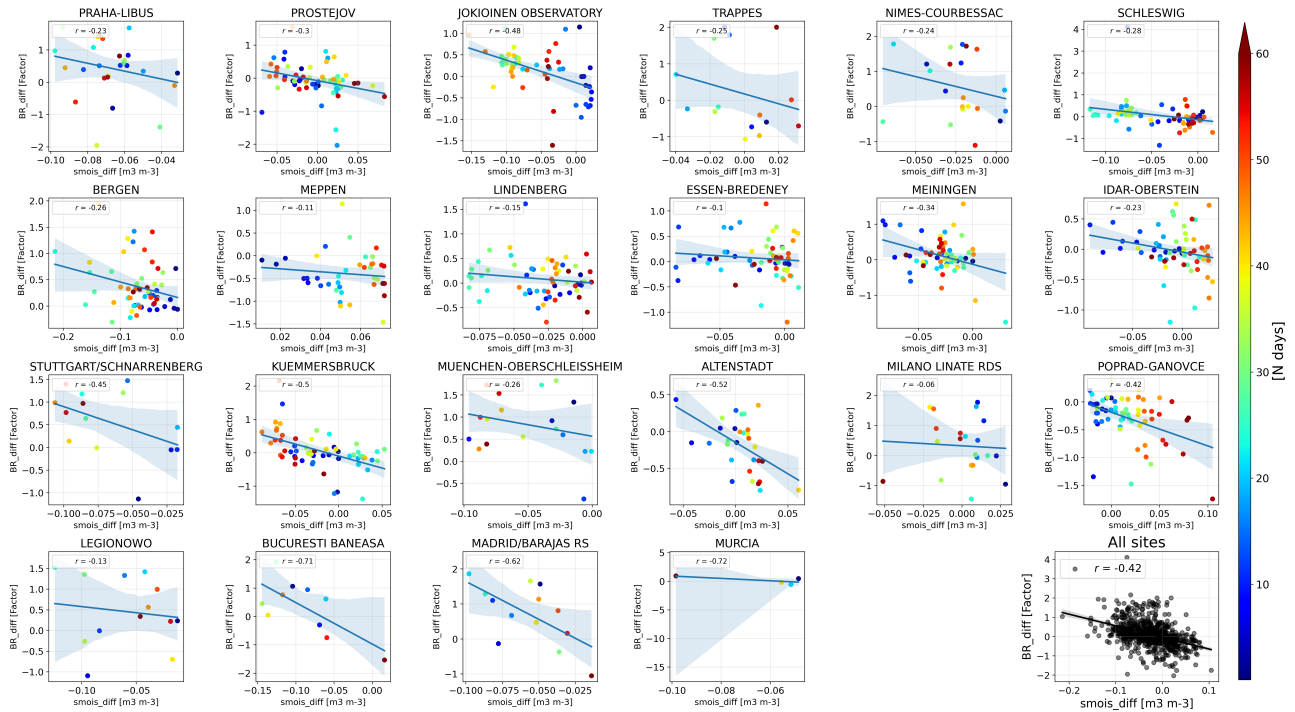


Figure S28. Scatter plot showing the correlation of the difference in SMOIS against the relative difference in Bowen ratio (BR) between simulation GN_DR and NN_NR at 22 different locations. The colors mark the day after 1 May (61 days in total up to 1 July) from blue to red. The plot in the lower right corner contains the data collected from all 22 sites.

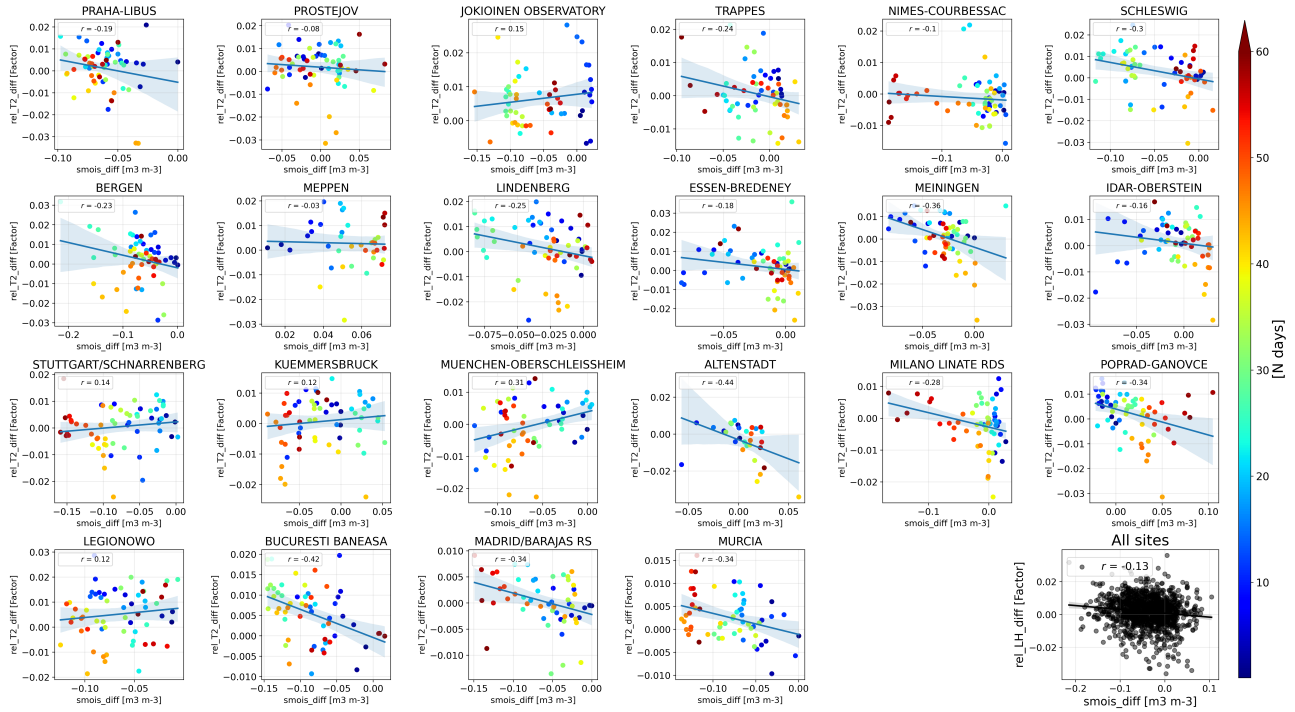


Figure S29. Scatter plot showing the correlation of the difference in SMOIS against the relative difference in T2 between simulation GN_DR and NN_NR at 22 different locations. The colors mark the day after 1 May (61 days in total up to 1 July) from blue to red. The plot in the lower right corner contains the data collected from all 22 sites.

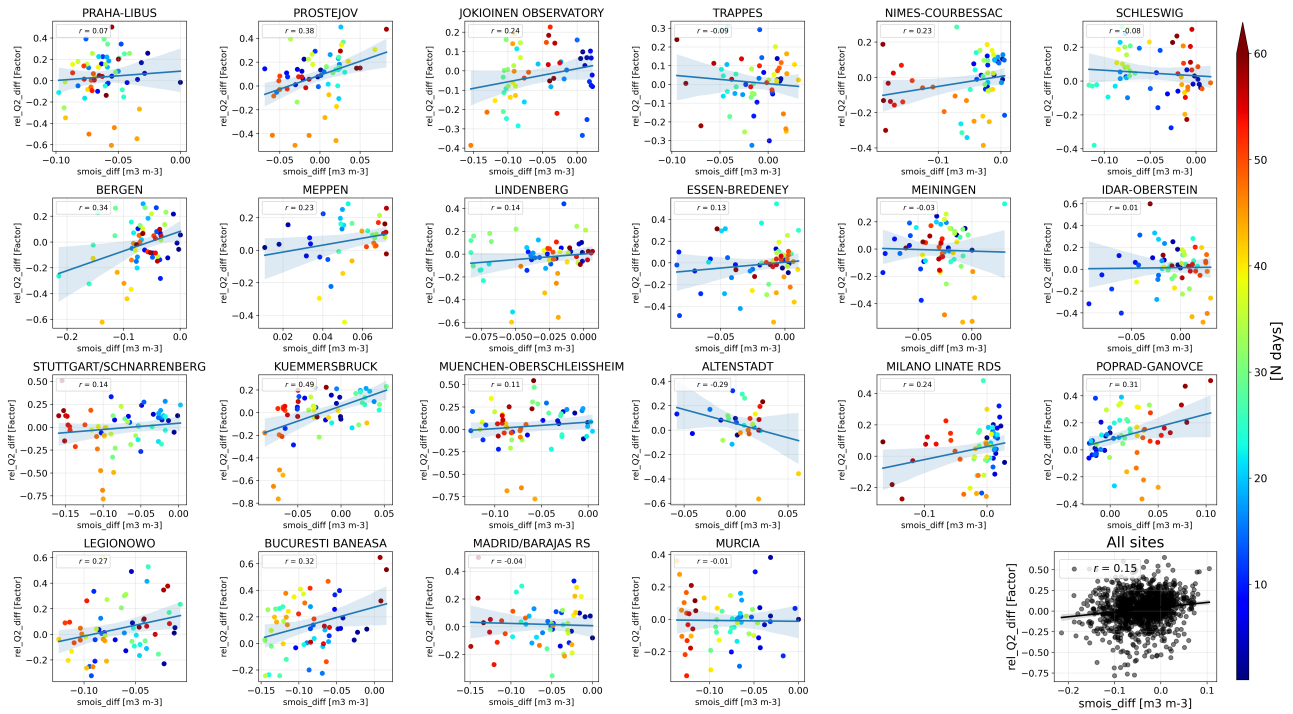


Figure S30. Scatter plot showing the correlation of the difference in SMOIS against the relative difference in Q2 between simulation GN_DR and NN_NR at 22 different locations. The colors mark the day after 1 May (61 days in total up to 1 July) from blue to red. The plot in the lower right corner contains the data collected from all 22 sites.

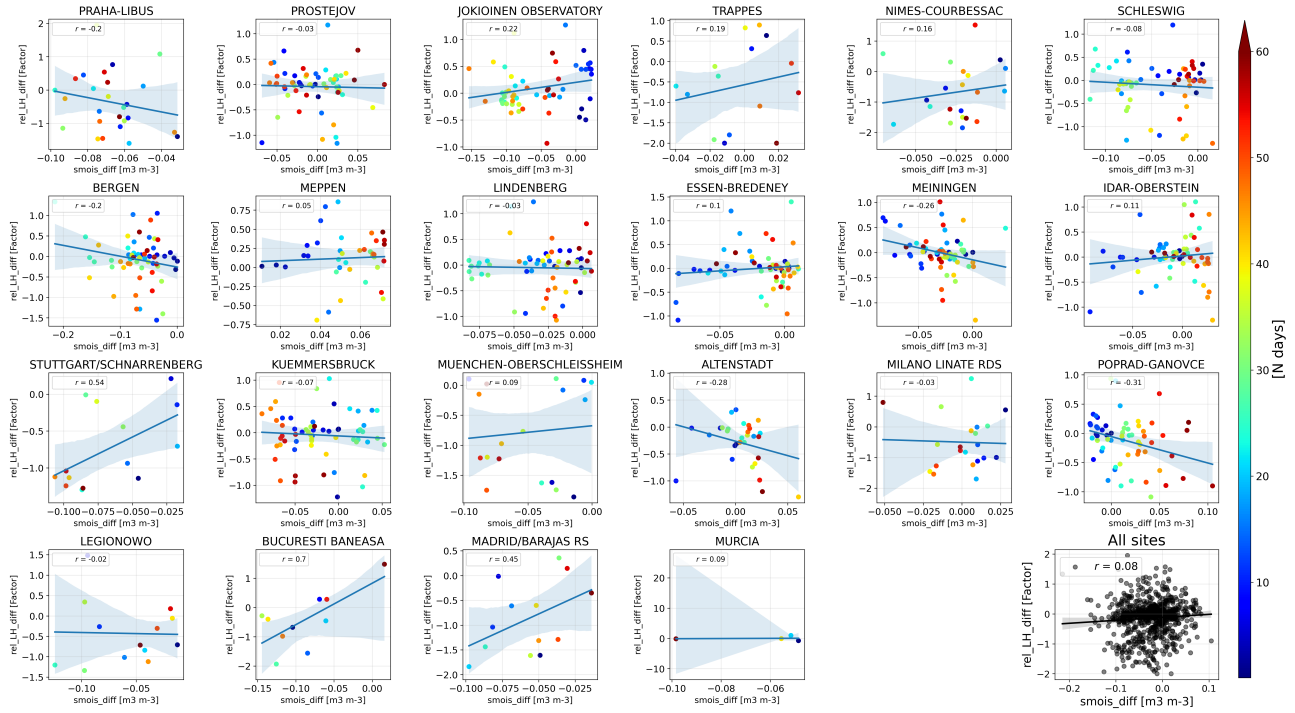


Figure S31. Scatter plot showing the correlation of the difference in SMOIS against the relative difference in Latent heat flux (LH) between simulation GN_DR and NN_NR at 22 different locations. The colors mark the day after 1 May (61 days in total up to 1 July) from blue to red. The plot in the lower right corner contains the data collected from all 22 sites. Note that due to the need to calculate the Bowen ratio (LH in the denominator), data points that lead the Bowen ratio to be N/A are removed.

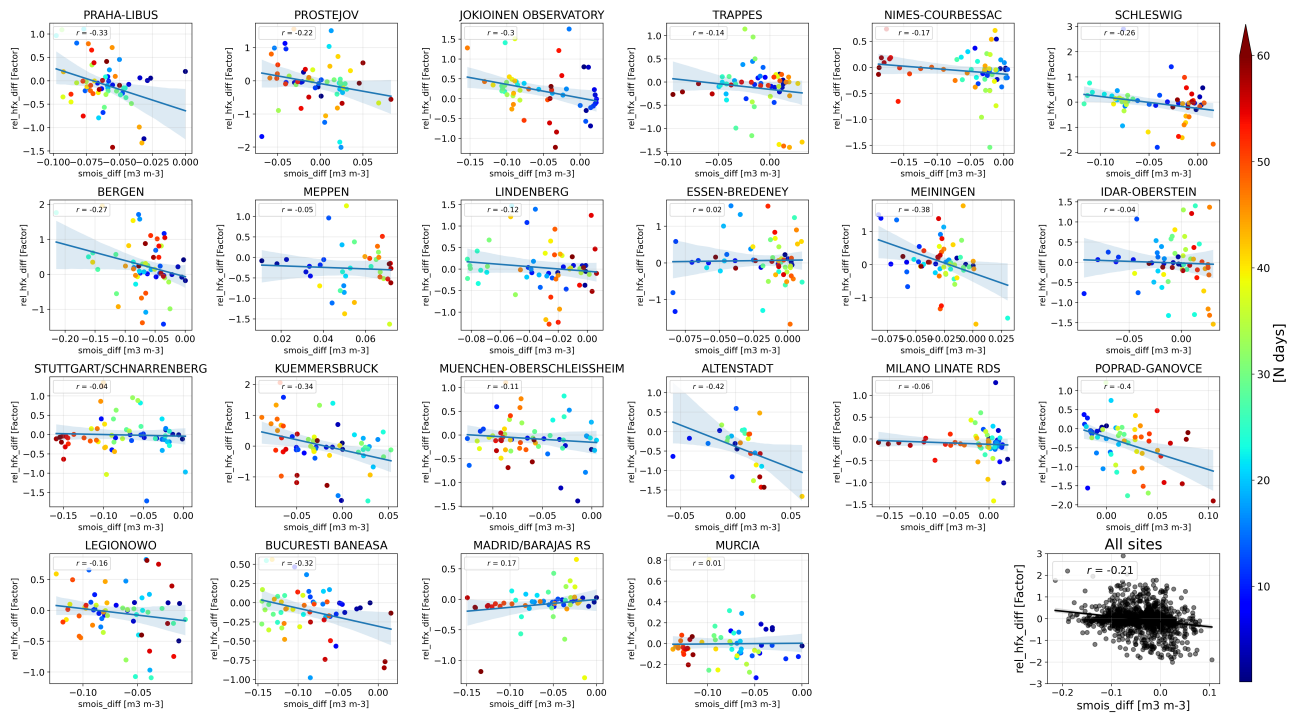


Figure S32. Scatter plot showing the correlation of the difference in SMOIS against the relative difference in Sensible heat flux (HFX) between simulation GN_DR and NN_NR at 22 different locations. The colors mark the day after 1 May (61 days in total up to 1 July) from blue to red. The plot in the lower right corner contains the data collected from all 22 sites. Note that due to the need to calculate the Bowen ratio (LH in the denominator), data points that lead the Bowen ratio to be N/A are removed.

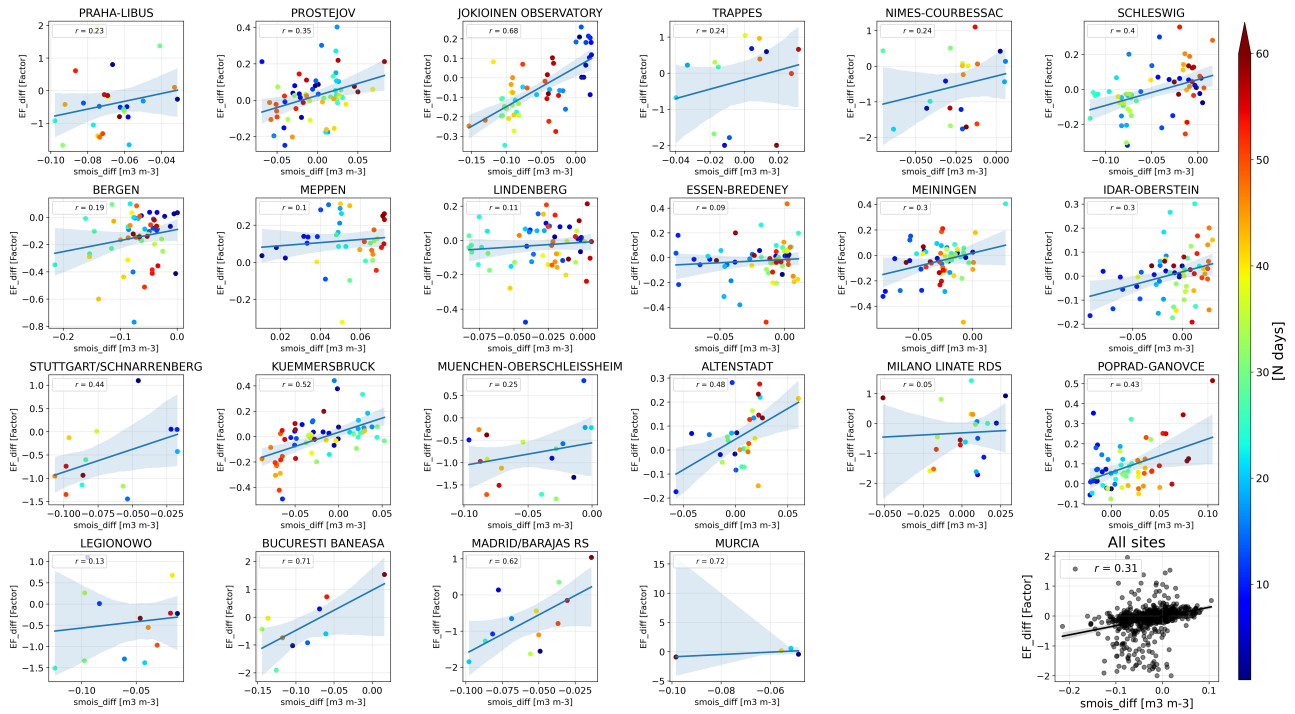


Figure S33. Scatter plot showing the correlation of the difference in SMOIS against the relative difference in Evaporative Fraction (EF) between simulation GN_DR and NN_NR at 22 different locations. The colors mark the day after 1 May (61 days in total up to 1 July) from blue to red. The plot in the lower right corner contains the data collected from all 22 sites.